A dual lane piezoelectric ring bender actuated nozzle-flapper servo valve for aero engine fuel metering

Michael Bertin[1], Andrew Plummer[1], Chris Bowen[1], Nigel Johnston[1], Mike Griffiths[2], Dan Bickley[2]

[1]Centre for Power Transmission and Motion Control, Department of Mechanical Engineering, University of Bath, BA2 7AY
[2]Rolls-Royce Controls and Data Services Ltd

Abstract
Amongst many other high performance flow control applications, servo valves are used to control aero engines by metering the fuel delivered from the fuel pump. Conventionally, a fuel metering servo valve has a pilot stage with an electromagnetic torque motor moving a flapper which differentially restricts a pair of nozzles to create a hydraulic signal (i.e. a pressure difference). These valve pilot stages use mature, optimised technology such that to achieve improvements requires a novel approach. Torque motors in particular present reliability and manufacturing difficulties, and news solutions should ultimately allow a reduction in manual assembly and set-up, improve repeatability, and eliminate failures associated with fine wire devices. In this paper, a pilot stage actuated by piezoelectric ring benders is proposed, designed, built and tested, and test results are compared with a model used to predict pressure-flow characteristics. A particular challenge is the need to include redundancy, and thus a pair of ring benders is used, allowing isolation between duplicated electrical control channels. Another challenge is the mounting of the ring bender, which has to flex to allow the outer edge of the ring bender to deform, yet be stiff enough to adequately react against generated forces. O-ring mounts made from three different elastomer materials are compared in this study. In aerospace, an added complication is the large range of fuel temperature; F70 fluorosilicone O-rings have been chosen with this in mind, and successfully demonstrated in the range -50°C to +180°C. With one active and one inactive ring bender to simulate a failure condition, the new dual lane pilot stage achieves +/-50µm displacement under test, giving control port flows up to +/-0.6L/min, and a control port pressure variation of 40bar using a 100bar supply pressure difference (supply minus return pressure). This research establishes that a piezoelectric aero engine fuel valve is feasible, and in particular, that piezoelectric ring bender actuators with elastomeric mountings are highly suited to this application.

1. Introduction

The world's passenger aircraft fleet will increase to 48 000 aircraft by 2037, more than doubling since 2018, requiring 37 000 new passenger and freighter aircraft according to Airbus' Global Market Forecast [1] Conversely, CO_2 emissions need to be reduced, so there is an urgent need to develop higher performance, more fuel efficient gas turbine aero engines.

An EHSV (electrohydraulic servovalve) is conventionally used to modulate the flow rate of fuel to the combustion chamber within an aero engine. The fuel metering valve has two stages: the pilot stage

and the main stage. The pilot stage of a conventional valve can be seen in Figure 1, consisting of a flapper moving between a pair of nozzles, actuated by an electromagnetic torque motor. A current amplifier is used to energise the coils and move the flapper to differentially restrict the two nozzles. The nozzle orifices form variable flow restrictors which are paired with fixed orifice restrictions to form an H-bridge as seen in Figure 2. P_S is the supply pressure from the fuel pump, and P_R is the pressure in the return line leading to the inlet of the fuel pump. The pilot stage controls two pressures, P_1 and P_2, which are applied to either end of a spool in the main stage of the metering valve, and it is the movement of this spool valve that regulates the size of the flow pathway through to the combustion chamber. The arrangement of the complete valve is shown in Figure 3. The main metering spool position is measured by an electrical sensor, such as an LVDT (linear variable differential transformer), and is used as feedback in a position closed loop, the controller within this loop determining the torque motor current.

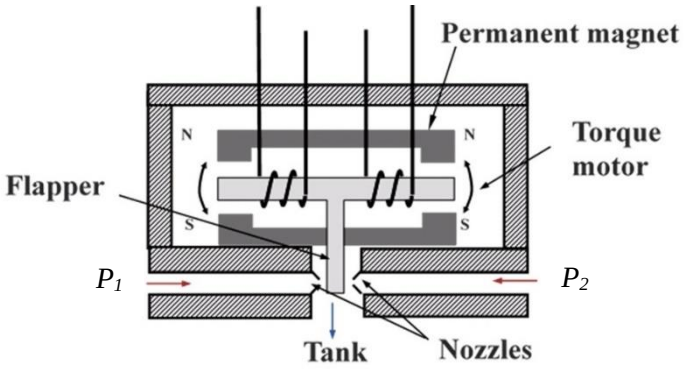

Figure 1. Conventional servo valve pilot stage: a nozzle flapper actuated by an electromagnetic torque motor

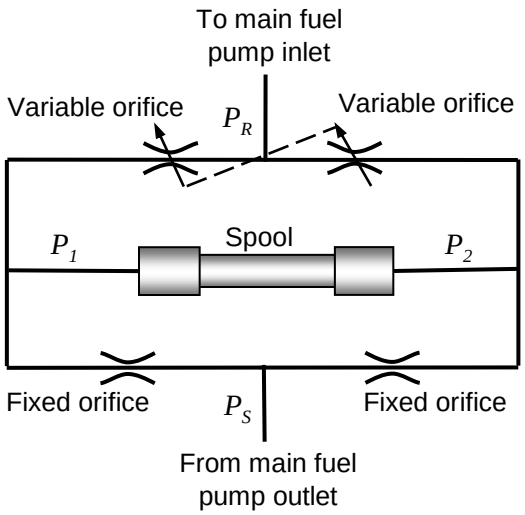

Figure 2. H-bridge orifice arrangement in fuel metering pilot stage

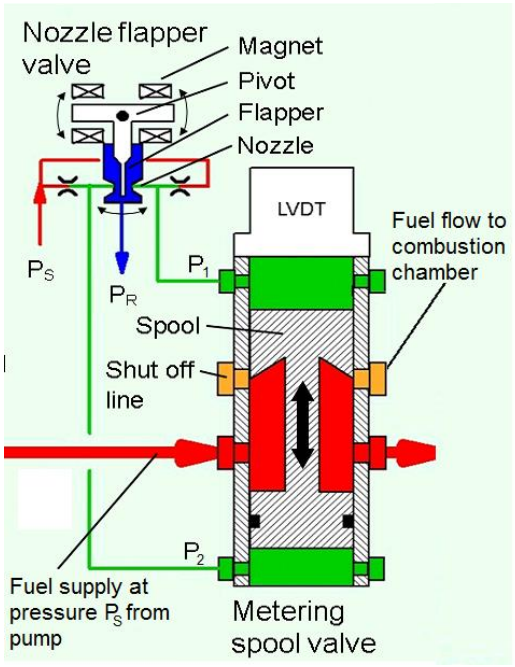

Figure 3. Fuel metering servovalve showing both pilot and main stages (adapted from [22]).

The torque motor actuated pilot stage has been used in its present form for half a century and its full development potential has probably already been reached [2]. In other applications such as in the automotive industry, fluid control systems employing piezoelectric actuation are starting to be introduced in order to increase performance [3]. A piezoelectric actuator might ultimately decrease production complexity and cost by allowing automated manufacture, which has proved unachievable with the conventional design. A torque motor uses fine wire electromagnet coils which, due to the manual nature of their production method, potentially have lower reliability and repeatability than a machine assembled component, and have high rejection rates. Also the large thermal stabilisation time required to settle the complex stack of electromagnetic components mitigates against rapid production. Once in service, the fine wire coils can be damaged by the high vibrations to which they are sometimes exposed, compounded by high levels of thermal cycling. They are also sensitive to contamination due to dirt ingress into the torque motor air gaps. Torque motors already make a significant contribution to the overall cost of aero engine fuel controls and with the anticipated increase in fuel system functionality on future platforms, the cost of pilot stage actuators will assume even greater significance.

Research into active combustion control in aero engines has necessitated high frequency fuel control which has also motivated investigation of piezoelectric actuation [4].

1.1 Piezoelectric actuation overview

Piezoelectric ceramics deform rapidly when an electric field is applied, but maximum strains are small, in the region of 0.15%. Lead zirconate titanate (PZT) is a ferroelectric ceramic commonly used for piezoelectric actuation, and by varying the ratio of lead zirconate to lead titanate, different compositions of PZT can be produced, displaying different properties. Composition can be placed into two general categories: ``Hard" and ``Soft" PZT. Hard PZT is characterized by small strain

capability compared with soft PZT, having limited domain motion, but can tolerate a large electric field and mechanical stress, and has a higher temperature limit and high Curie temperature before depolarisation. Hard PZT ferroelectrics also exhibit low hysteresis, due to restricted domain motion.

Due to the small strain output, direct actuation using a multi-layer stack of piezoceramic plates (Figure 4a) is likely to be impractical even for the small displacement range needed in the pilot stage flapper (typically 0.1mm). Rectangular bending actuators, such as that shown in Figure 4b, can provide sufficient displacement at reduced force compared to a stack. Ring bender actuators, such as those in Figure 4c, which have only become widely commercially available relatively recently, provide sufficient displacement for pilot stage actuation, at reasonable force levels (in the region of 10N to 100N) [5]. Multi-layer ring benders are available with ceramic layers as thin as 20μm, in which case applied voltages of approximately 50V provide sufficient field strength for maximum displacement. Disadvantages of piezoelectric actuation using ferroelectric materials include their hysteretic behaviour (typically 20%), creep, and the temperature dependence of stack actuator length [6]. Piezoelectric actuators are electrically similar to capacitors, so speed of response is generally constrained by the amplifier current limit.

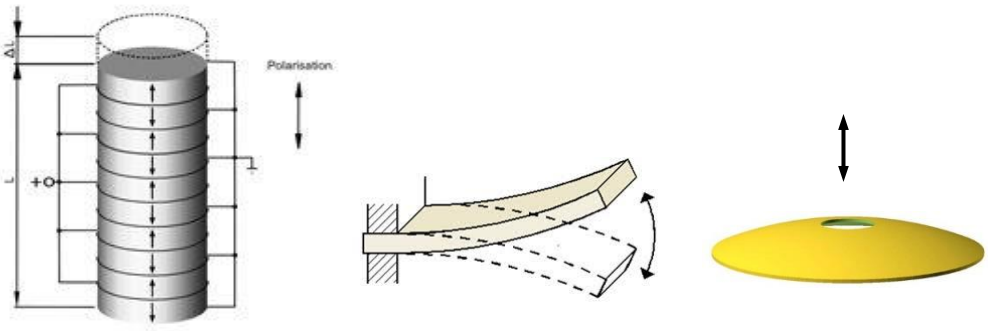

(a) Axial actuator (stack (b) Rectangular bender (c) Ring bender

Figure 4. Common piezoelectric actuators

1.2 Piezoelectric actuation of valve pilot stage

The concept of actuating a servovalve using piezoelectric ceramics is not new. In a 1955 valve survey [7], it was noted that "piezoelectric crystals have been used on certain experimental models to obtain improved response", and proceeds to say that "they have not been accepted to date because of high susceptibility to vibration, temperature changes, and electrical noise and because of the difficulty in obtaining sufficiently large displacements from the crystals". A patent for a piezoelectric valve was also filed in 1955, covering both a piezo-actuated flapper for a double nozzle-flapper valve, and also delivering fluid using an oscillating piezo-disc i.e. a piezo-pump [8]. Piezo-actuated hydraulic servovalve research since the 1950's is included within the reviews of Tamburrano *et al* [9] and Plummer [10].

Replacing the torque motor in a two-stage valve with a piezoelectric actuator was reported in a number of studies. Karuanidhi and Singaperumal [11] presented a servovalve where a flextensional actuator (a stack in a flexing frame providing motion amplification) actuates a flapper in a mechanical feedback valve, see Figure 5. An aerospace servovalve, again with a feedback wire, was presented by Sangiah *et al* [12]. This used a rectangular piezoelectric bender to move a deflector jet, arguing that the smaller flow forces experienced in a deflector jet (or jet pipe) pilot stage compared to a nozzle-

flapper are more suited to bender use, see Figure 6. In comparison with a torque motor, it was suggested that a piezoelectric bender may prove easier to manufacture and commission, and provide more repeatable performance. Milecki also developed a servovalve with a rectangular bender actuated pilot stage, this time in a nozzle-flapper arrangement and using electrical feedback of the spool displacement [13]. The bender was capable of producing a maximum displacement of +/- 0.08mm and force of 2N with a +/- 30V supply voltage. However the author reported that the valve exhibited stability problems, and was significantly affected by actuator hysteresis.

In a recent valve prototype, a ring bender was used as the pilot stage actuator [14-16]. This time the pilot stage was a miniature spool with some overlap used to minimize pilot stage leakage flow. Electrical spool position feedback was used, see Figure 7. Figure 8 shows a pilot operated piezoelectric valve with two adjustable restrictors described by Hagemeister [17], and Bauer and Reichert [18]. The pilot stage used a pair of single nozzle-flappers to control the pilot pressures on each side of the spool separately. The 'cross-bow' benders (rectangular benders pinned at each end) actuating the flappers have a fairly small force output (<10N) so the nozzle flow forces were reacted using compensating pistons fed by the pilot pressures. The dynamic response was good with a -3dB bandwidth at 550Hz with 20% amplitude. A similar concept was investigated by Tamburrano *et al* via detailed modelling studies [19,20]. A piezo-stack actuated pilot stage concept was described by Reichert and Murrenhoff [21]. As shown in Figure 9, all four orifices in the pilot stage H-bridge were modulated using stack actuators from designed for automotive fuel injectors with 40μm stroke (free displacement), and a -90° bandwidth of over 1kHz was achieved.

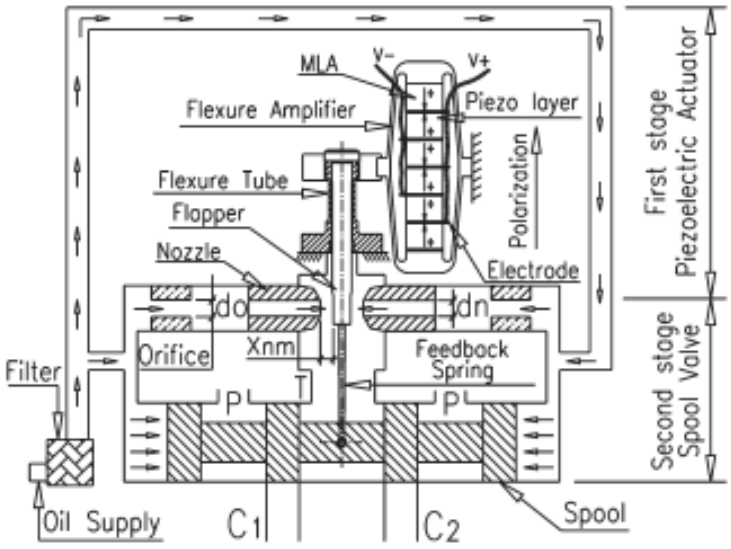

Figure 5: Piezoelectric stack with flex-tensional amplification for two-stage valve [11]

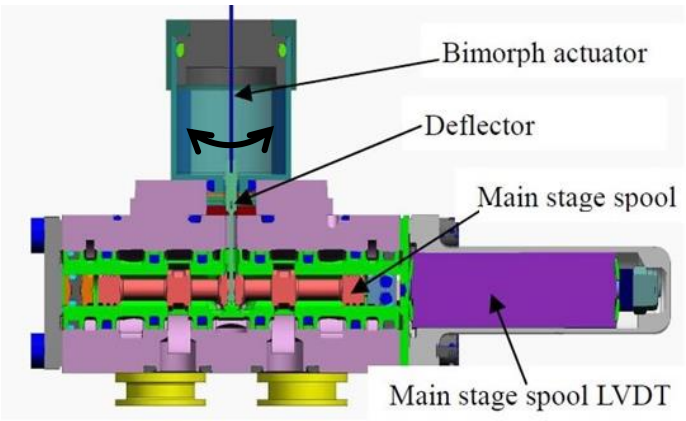

Figure 6: Piezoelectric rectangular bender deflector jet two-stage mechanical feedback valve (described in [12]).

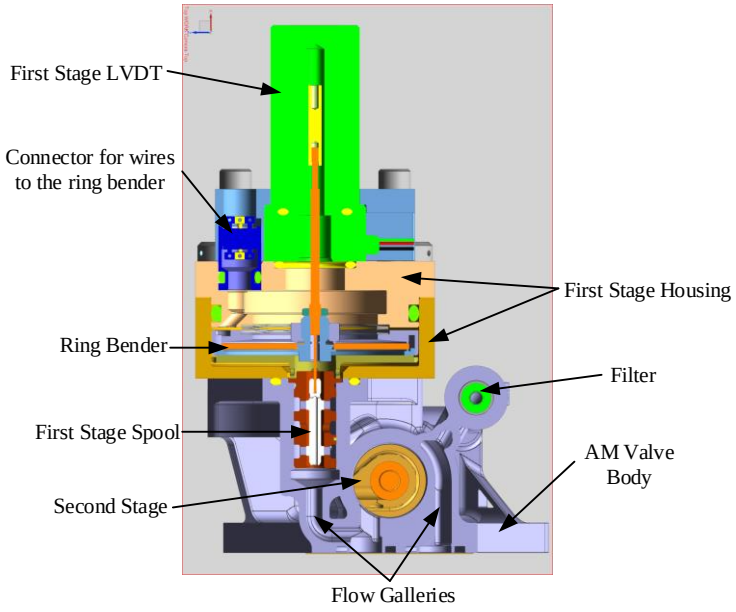

Figure 7: Piezoelectric ring bender actuated pilot spool in two-stage electrical feedback valve (described in [15]).

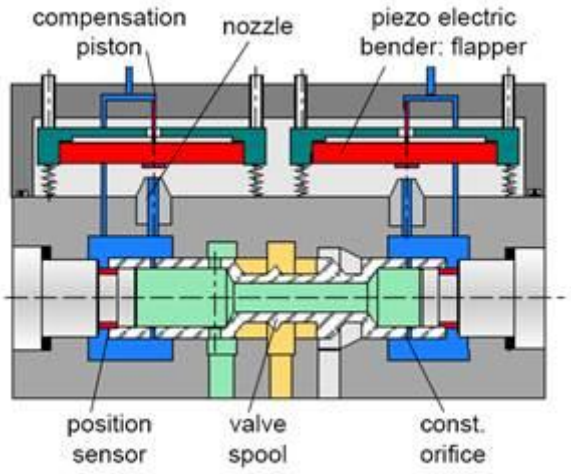

Figure 8: Piezoelectric bender valve with individually controlled nozzles [18].

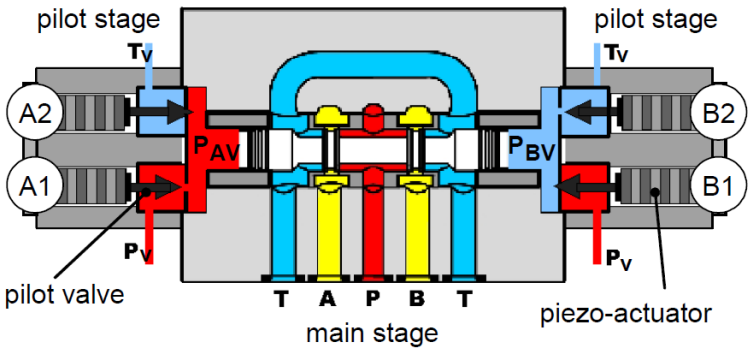

Figure 9: Independent piezo control for pilot stage H-bridge orifices [21].

In summary, a number of concepts for piezo-actuated pilot stages have been researched for use in two-stage servo valves, i.e. servo valves in which the displacement of the main spool is caused by a difference in fluid pressure across its end-faces. The pilot stage is responsible for generating this pressure difference. Direct drive piezo-actuated spool valves have also be investigated by several researchers, see e.g. [9], but the displacement range (typical ±1mm), force and speed requirements are very challenging. Thus only pilot stage actuation is considered here. A comparison of the designs which have been reviewed is contained in Table 1.

Reference	**Pilot stage piezo actuation concept**	**Comments**
[11] Figure. 5.	Flex-tensional nozzle-flapper valve	An issues with this design is that the suspended mass of the stack in the flex-tensional amplifier will make the pilot stage sensitive to external vibration; likewise, the mass and compliance of the actuator limit the dynamic response. Also the asymmetrical design is likely to give thermal sensitivity issues.
[12] Figure 6.	Cantilevered rectangular bender driving deflector jet valve	The limited force of the rectangular bender is only likely to be suitable for the more expensive deflector jet hydraulic amplifier, due to the smaller flow force compared to a nozzle-flapper.
[15] Figure 7.	Ring bender moving a miniature spool	Higher force output of ring bender is generally well suited to pilot stage actuation, but not high enough to prevent the miniature spool jamming in the presence of fluid contamination (i.e. does not provide sufficient chip shear force). Friction and cost are other problems (Plummer, 2016).
[17] Figure 8.	Pair of single nozzle-flappers with 'cross-bow' rectangular benders	Benders pinned at each end give higher force than cantilevered rectangular bender, but typically less than similar-sized ring bender. Reliably compensating for supply pressure changes is challenging with single nozzle-flappers
[21] Figure 9.	Independent control of all 4 H-bridge orifices using stacks.	A high performance but complex and expensive arrangement, requiring 4 sets of actuators and drive amplifiers. High frequency operation limited by self-heating and high power demand / low efficiency. Leakage found to be a high, and pilot stage flow is limited by small stack displacement.

Table 1. A comparison of piezo-actuated servo valve pilot stage designs.

1.3 Multi-layer piezoelectric ring bender for flapper actuation

A piezoelectric ring bender is a circular piezoelectric actuator with a central hole. Several thin piezoceramic layers are usually used, interspersed with electrodes. The layers are poled so that the top layers deform in opposition to the bottom layers when a voltage is applied. The electric field direction is across the thickness of the ring bender, which causes the layers to deform in the radial and circumferential directions via the piezoelectric d_{31} mode. As a result, the ring bender deflects at right angles to the plane of the disc such that it forms a dome shape; the direction of deflection depends on the sign of the voltage. Thin piezoceramic layers are used so that the maximum field strength (about 3kV/mm for PZT) can be reached at a low voltage. The three-wire parallel electrode connection is preferred, which is illustrated using just two layers in Figure 10, as the field direction never opposes the poling direction, and this maximises allowable field strength and hence also gives a larger range of displacement. A ring bender actuator exhibits a greater displacement than a stack actuator of the same mass, and an increase in stiffness in comparison to a similar sized rectangular bender. The range of displacement and force make it highly suitable for actuating a flapper in a nozzle-flapper valve pilot stage.

This paper presents the development and testing of a novel double nozzle-flapper type servo valve pilot stage actuated by a piezoelectric ring bender actuator, including comparison with an analytical model. The ring bender is mounted by flexibly clamping its outer edge, and attaching a hub at its centre which moves between two nozzles, thus taking the place of the flapper. In safety-critical aerospace control applications, "dual lane control" is required for redundancy, meaning the nozzle flapper must be drivable by two separate actuators. The novel valve presented here can be configured in single lane and dual lane modes whereby either one or two ring benders are attached to the moving hub.

In comparison with actuators used in the previous designs summarised in Table 1, a ring bender is a light and compact actuator providing a combination of force and displacement ranges which is very suitable for this application. High performance multi-layer ring benders have only become commercially available in the last few years, and only used previously in a servovalve application by Persson *et al* [15]. However, unusually, the pilot flow in Persson's valve is controlled by a miniature spool, and for which driving actuator would normally be expected to be able to supply a high 'chip shear force' (typically ~100N) to prevent jamming by contaminant particles in the fluid, which is not easy to achieve with a ring bender. Hence the design in the present work uses the more conventional nozzle-flapper pilot stage arrangement, which also gives the advantages of low friction, and improved damping of the main spool movement at low velocity. For the aeroengine fuel metering application, reliable operation over a wide range of temperatures is important and this issue is considered in this paper. Section 2 presents the design of the prototype valve, and a model for predicting the valve characteristics is derived in Section 3. Experimental results under different flow and pressure conditions are shown in Section 4. These are compared with predictions from the model. Further considerations and conclusions on the use of piezoelectric ring benders for this application are discussed in Section 5.

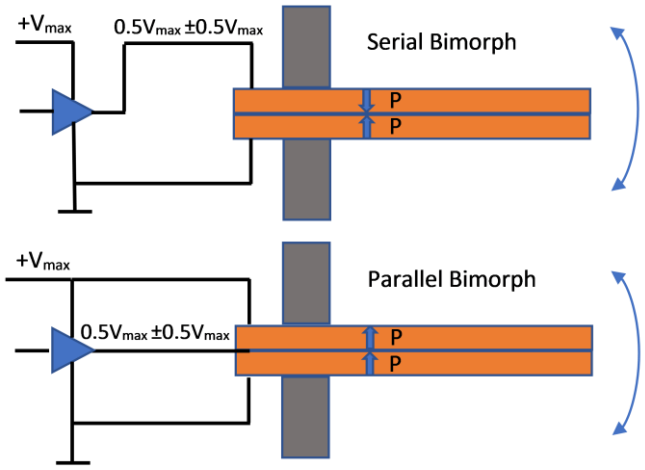

Figure 10. Alternative electrical excitation arrangements for bending actuators

2. Experimental piezoelectric pilot valve and test system

2.1 Pilot valve prototype

A prototype ring bender actuated nozzle-flapper valve pilot stage was designed and built. Figure 11 shows the valve set-up in dual lane mode, i.e. with two ring benders mounted in the valve. The labelled parts correspond to the picture of the components in Figure 12. The arrows show the flow path through the left hand nozzle; a symmetrical flow path also exists through the right hand side. The valve was manufactured in stainless steel (grade 431) and the design was intended to be sufficiently stiff to withstand high pressure with minimal deformation. The ring bender mount and the valve outer body were designed to be separate so that multiple actuator configurations could be tested, particularly single and dual lane. The nozzle axial positions were designed to be adjustable to allow for different orifice clearance, dependent on the test set-up.

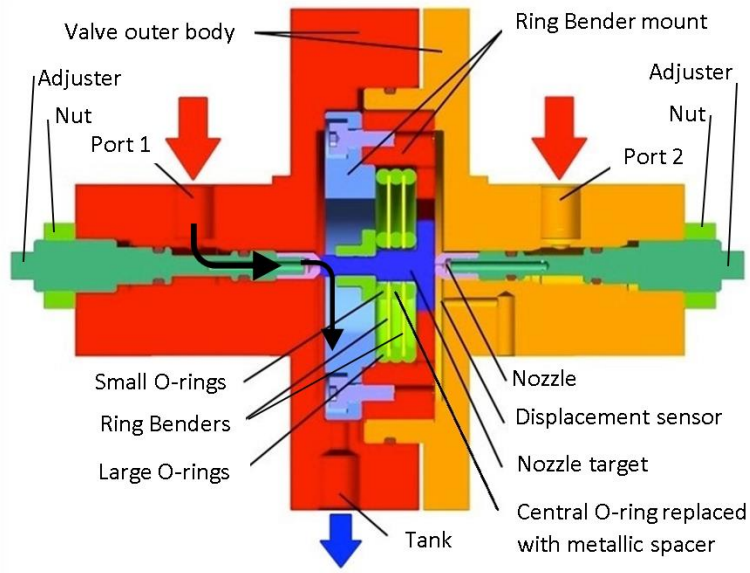

Figure 11. Experimental valve pilot stage in dual lane arrangement.

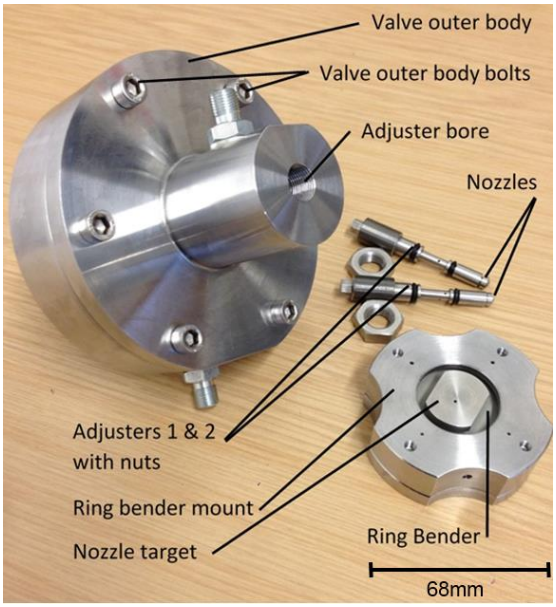

Figure 12. Components of the experimental valve.

The prototype is dimensioned in line with an existing commercial fuel valve. This has a full bi-directional stroke of 152µm, giving 76µm clearance from each nozzle in the centre position [22]. A force of at least 5N has to be available to move the flapper, not only to overcome flow and pressure forces but also to drive through contaminant particles that may block the flow path through the nozzles [22].

These two criteria, displacement and force, were used to select the Noliac CMBR07 as the most appropriate off-the-shelf commercial ring bender. The characteristics of this ring bender are summarized in Table 2. Figure 13a shows the ring bender and Figure 13b is a cross-section view of the internal structure (perpendicular to the plane of the disc, about midway between the inner and outer edge), with the electrodes labelled. The electrode labels are colour coded to match the wire colours in Figure 13. The ring bender is manufactured from a soft PZT piezoelectric ceramic, NCE57, which has properties similar to well-known materials such as PZT-5A. The internal structure is comprised of 10 layers of NCE57, each 67µm thick, separated by internal electrodes. The Curie temperature, above which the material is fully depolarised, is 350°C for NCE57. The specified operating temperature range in the aero engine environment is -50°C to 180°C [22].

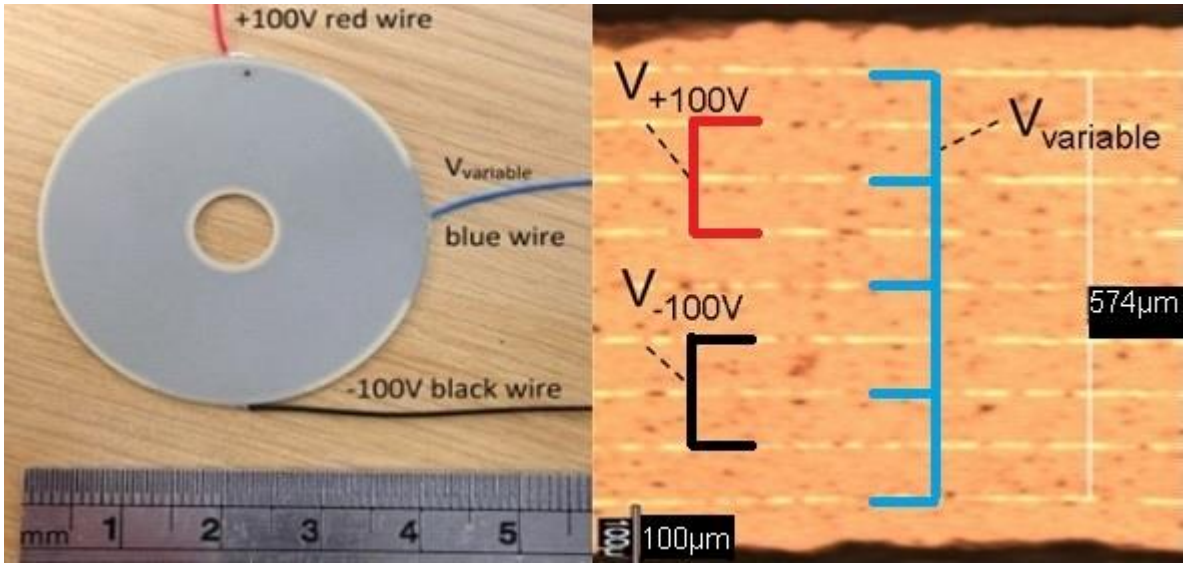

Figure 13.{a) Image of a typical ring bender CMBR07. b) Optical microscopic section view of the ring bender showing the ceramic layers and electrodes.

Table 2. Properties of Noliac ring bender CMBR07

Outer diameter	40mm
Inner diameter	8mm
Thickness	0.67mm
Free Displacement (maximum no load displacement)	±185µm
Blocking Force (maximum force at zero displacement)	13N
Drive voltage	±100V

In dual lane mode, to achieve redundancy two ring benders are mounted flexibly by clamping between three large diameter elastomeric O-rings at their outer edges, numbered 1-3 in Figure 14. The hub, providing the nozzle target, is attached via two small diameter O-rings around the inner edges (4,6), and a metal spacer between the two benders (5). It is particularly important to mount the ring benders flexibly at their outer edge or else their free displacement is significantly reduced, but too much compliance reduces the blocking force. In this case, the mount is designed such that the compression of the outer O-rings gives a clamping force of approximately 75N.

In order to equalise the pressure in the volume trapped between the pair of ring benders with the return pressure present outside the pair, a metallic inner edge spacer ring (5 in the Figure) was used in which breather holes were cut. These connected with breather passages in the target.

A Noliac amplifier, model no. NDR6110, is used to drive the ring benders, providing constant +100V and -100V outputs, and a variable control voltage varying between these two values. The variable amplifier output voltage was monitored during testing. To measure the displacement of the nozzle target, a Microepsilon eddy current sensor was used, labelled in Figure 11. The range of the sensor is 500µm and the resolution is 0.025µm.

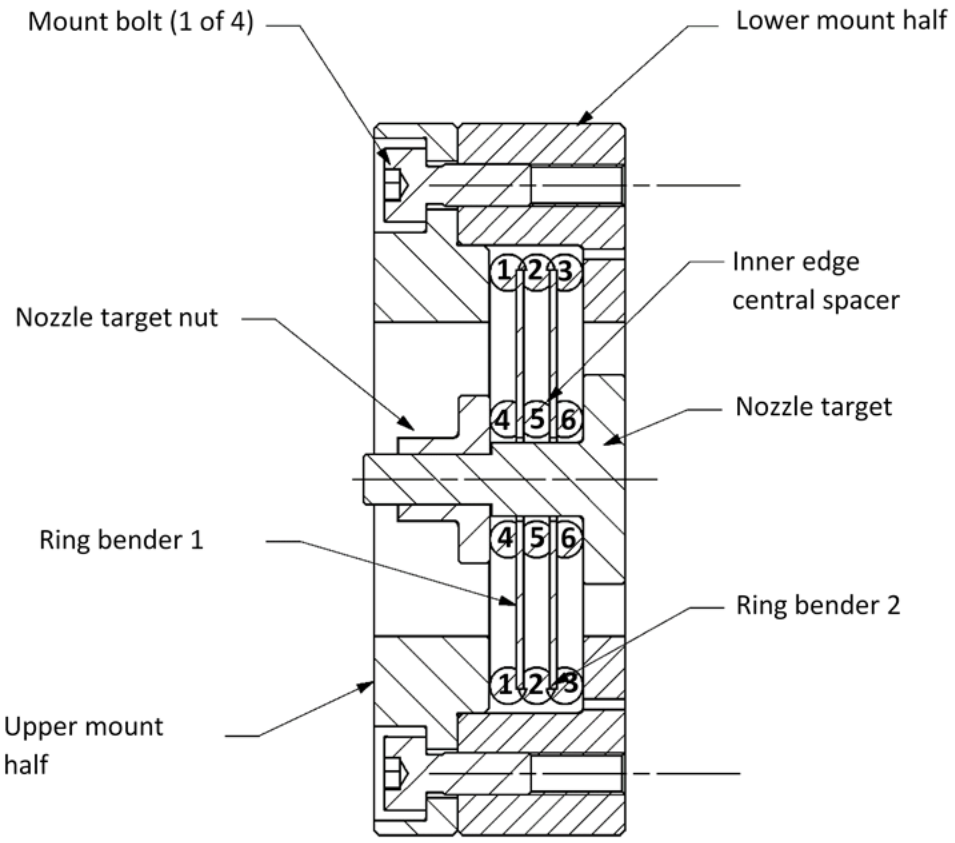

Figure 14. Ring bender mounting with the dual lane set-up. Fluorosilicone O-rings are numbered 1-4 and 6; 5 is a metal spacer ring.

2.1 Ring bender mounting details

The outer edge mounting O-ring was selected to approximately overlap the outer 1mm of the ring bender and in doing so insulate the electrodes at the outer edge. The inner edge mounting O-ring was selected such that the internal diameter was great enough for the hub/target to fit through the ring bender central hole with minimal clearance. A pre-compression of 75N was used for all mountings.

There are several environmental requirements for the O-ring material in this application, particularly related to fuel compatibility and temperature range. Nitrile, fluorocarbon and fluorosilicone O-rings were compared. Specifications of the mounting O-rings are shown in Table 3. It is know that Nitrile is unlikely to be appropriate due to the high fluid temperatures expected. F70 fluorosilicone is much more stable over the required temperature range, but absorbs fuel and swells over time. The 3480 grade fluorocarbon will absorb less fuel but the glass transition point for the fluorocarbon material is close to the minimum of the specified temperature range.

Figure 15 compares the measured compressive displacement of the three outer edge elastomer O-rings under compressive load. Nitrile and fluorocarbon have the largest stiffness and fluorosilicone is notably less stiff. As can be seen in Figure 16, which is a test with a single ring bender, the fluorosilicone O-ring inhibits the motion of the ring bender more than the fluorocarbon at room temperature. The mounting force was the same (75N) in both cases for this comparison, and the reduction in displacement is caused by the larger contact region which results with the more compliant fluorosilicone O-ring, as it needs to be compressed more to achieve this mounting force. The piezoelectric hysteresis is clearly visible in this plot.

Table 3. Dimensions and characteristics of elastomer O-rings.

Parameter	**Nitrile**	**Fluorosilicone, F70 (Fairway Seals)**	**Fluorocarbon, 3480 (Trelleborg)**
Outer edge dia.	37.7mm	37.47mm	37.7mm
Outer edge thickness	3.5mm	3.53mm	3.5mm
Inner edge dia.	8mm	7.52mm	8mm
Inner edge thickness	3.5mm	3.53mm	3.5mm
Shore A hardness	70+/-5	70+/-5	75+/-5
Temperature range	-35ºC to 110 ºC	-60 ºC to 177 ºC	-51 ºC to 204 ºC
Glass transition	-	-60 ºC	-51.7 ºC
Compression set, 22 hours at 175 ºC.	-	12.78%	8.0%
Volume change in oil for 70 hrs at 200ºC	-	+21.47%	+7.2%

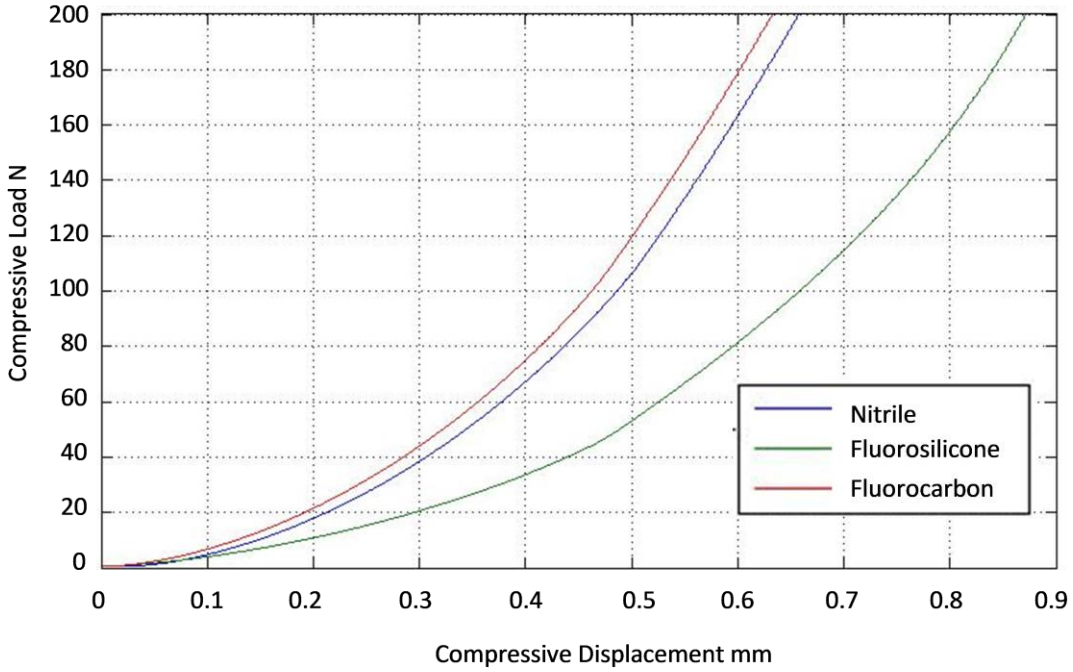

Figure 15. Compressive force with displacement for Nitrile, Fluorosilicone and Fluorocarbon O-rings.

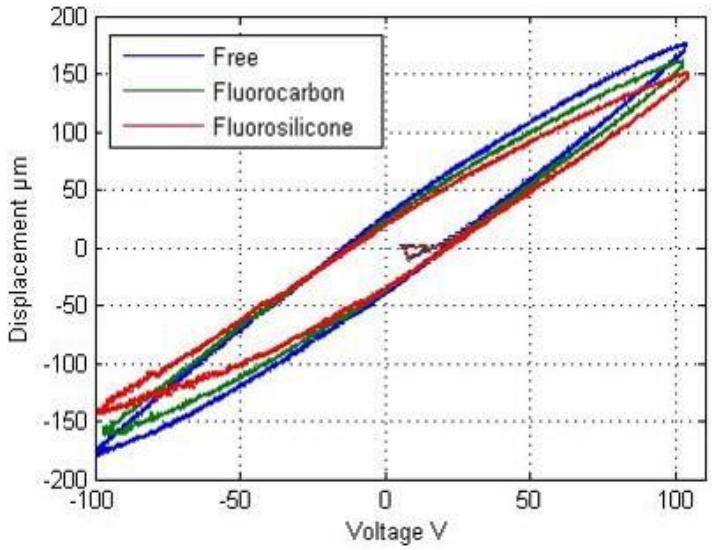

Figure 16. Comparison of ring bender displacement when unmounted, and when the outer edge is mounted between of O-ring pairs with 75N pre-compression.

For this application, operation over a wide range of temperatures (-50°C to +180°C) is required. Figure 17 compares the free displacement of the ring bender when unmounted with the free displacement when the ring bender is mounted between fluorosilicone and fluorocarbon O-rings over this range of temperatures. At each temperature, the ring bender is driven similarly to Figure 16, with a sinusoidal voltage of +/-100V applied at 1Hz, and the peak positive and negative displacements are averaged. Note that the displacement of the free ring bender is temperature dependent, a result consistent with previously published results [23]. As already noted, the fluorosilicone mounting reduces the displacement the most at room temperature, by 17% versus 8% reduction with the

fluorocarbon mounting. However below -30°C the fluorocarbon begins to transition to a glassy state and displacement drops rapidly, so it would not be suitable for the entire temperature range. As a result of these measurements, the fluorosilicone mounting is used for all results presented in the rest of the paper.

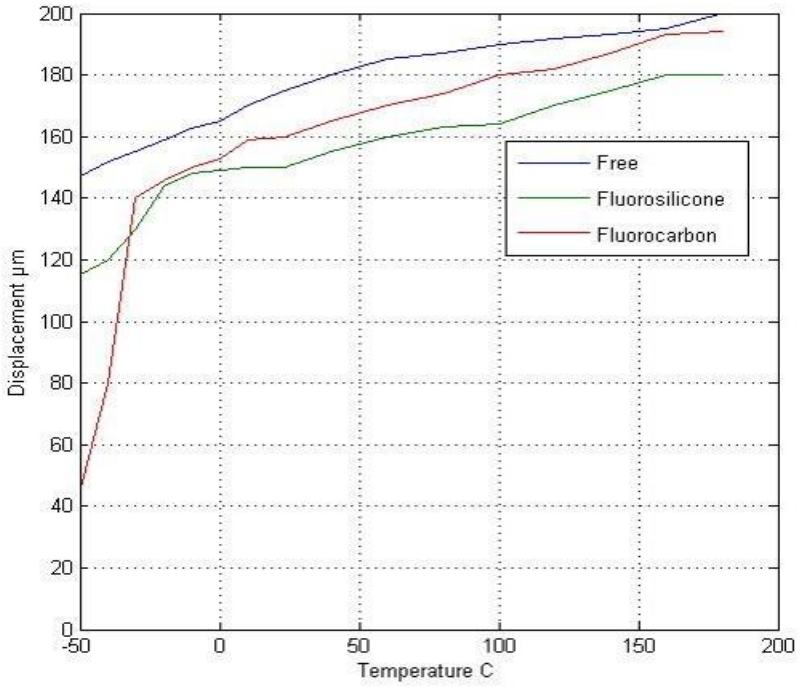

Figure 17. Maximum displacement of a ring bender with alternative mountings plotted against temperature

2.3 Test circuit

The hydraulic circuit used to test the pilot valve can be seen in Figure 18, including needle valves which are used to form the two fixed restrictions in the H-bridge (left hand side of Figure 18). A pressure control valve is used to keep the supply pressure from the pump constant. The maximum supply pressure used in these tests was 110bar. A restrictor is used in the return flow path to tank so that pressure P_R can be raised above atmospheric pressure to reduce cavitation in the valve. Piezoresistive pressure transducers (PT) are used to record the pressure at each of the two control ports, P_1 and P_2, as well as the supply and return pressure. The fixed restrictions are set such that the control port pressures are half the supply pressure when the nozzle target is in the null (i.e. central) position. Fluid temperature is recorded and tests are conducted at constant temperature. Hydraulic oil (ISO grade 32) was used as a substitute for aero engine fuel to reduce fire risk. Figure 19 is a photo of the test setup.

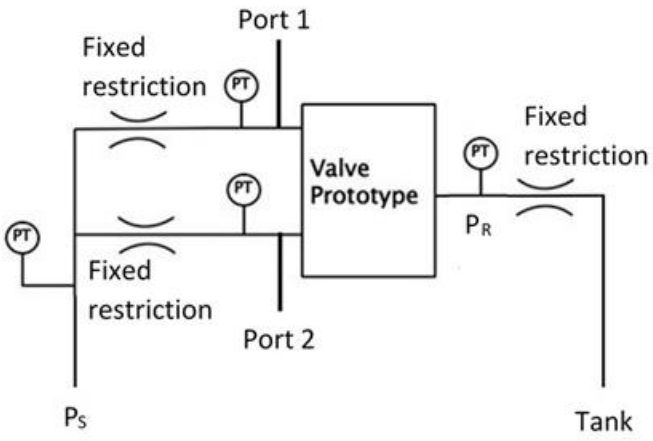

Figure 18. Hydraulic circuit (PT is pressure transducer)

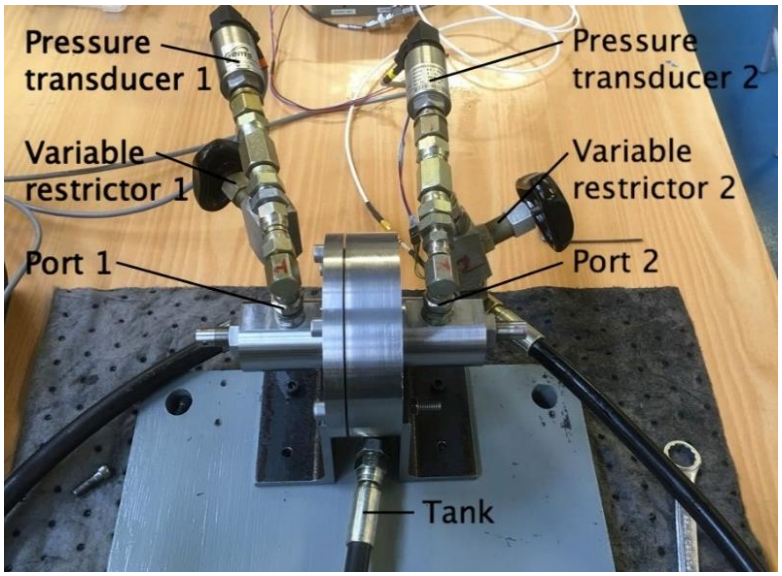

Figure 19. Prototype valve test set-up in blocked port mode (ports 1 and 2 blanked).

3. Model of valve pressure-flow characteristic

The theoretical relationship between the valve outlet pressure or flow and the voltage applied to the ring bender is derived in this section. The relationship is consistent with models of conventional nozzle-flapper valves [24]. and also other research into piezoelectric servo valves [12.25]. Figure 20 illustrates the notation for pressures, flows, and orifice dimensions used in the model. Two situations are considered:

- blocked port mode, in which there is no flow to control ports 1 and 2
- connected port mode, in which the control ports are connected and so that the two flow rates are equal but of opposite sign.

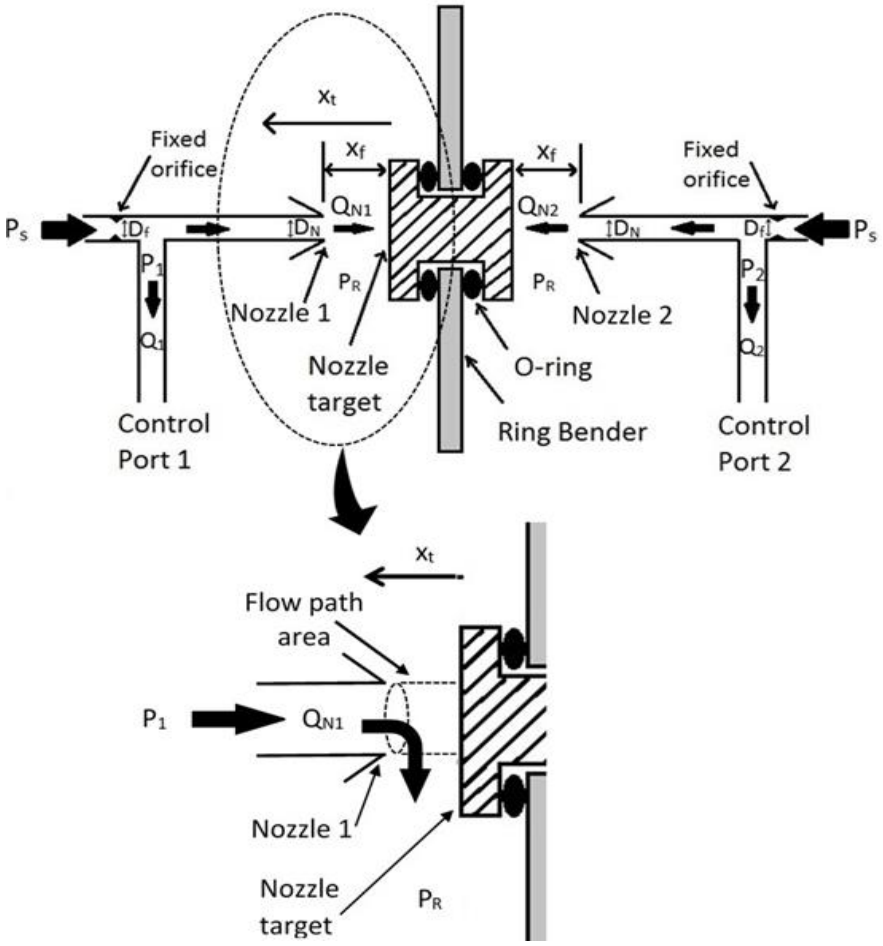

Figure 20. Pressures, flows and dimensions used in model (shown with single ring bender)

3.1 Simplified ring bender model

The ring bender model was simplified to a linear relation between displacement ($\hat{x}_t$), voltage (V) and force (F_N):

$$\hat{x}_t = k_1 V - k_2 F_N \tag{1}$$

subject to the constraints of working within the clearance between the flapper and the nozzle (x_f):

$$x_t = x_f \;\; if \;\; \hat{x}_t > x_f$$

$$x_t = -x_f \;\; if \; \hat{x}_t < -x_f$$

$$x_t = \hat{x}_t \;\; if \;\; -x_f \leq \hat{x}_t \leq x_f$$

In the results presented later, the model is parameterised for a dual lane arrangement with one active ring bender and a second inactive open circuit ring bender. The values k_1 and k_2 are experimentally derived based on the measured displacement and force in this dual lane arrangement. Ring bender hysteresis is not included, although various models could be used to represent it, such as presented in [26].

3.2 Hydraulic model

A simplified hydraulic model is used in which fluid compressibility is not considered. The flow-pressure relationship for a nozzle or a fixed restrictor can be described by the orifice equation:

$$Q = C_q A \sqrt{\frac{2\Delta P}{\rho}} \tag{2}$$

where Q is flow through the orifice, A is the area of the orifice, ΔP is the pressure difference across the orifice, ρ is the density of the fluid (oil) and C_q is the flow coefficient.

Considering nozzle 1, as the cross-sectional area of the orifice varies with the position of the nozzle target, the flow through nozzle 1 can be expressed as:

$$Q_{N1} = C_v \pi D_N x_{N1} \sqrt{\frac{2(P_1 - P_R)}{\rho}} \tag{3}$$

where,

$$x_{N1} = x_f - x_t \tag{4}$$

and C_v is the flow coefficient for the variable orifice, and D_{N1} is the nozzle diameter.

Or rearranging:

$$P_1 - P_R = \frac{Q_{N1}^2}{K_v x_{N1}^2} \tag{5}$$

where,

$$K_v = \frac{2C_v^2 \pi^2 D_N^2}{\rho} \tag{6}$$

is a constant for the variable orifice. For the fixed orifice:

$$P_S - P_1 = \frac{(Q_1 + Q_{N1})^2}{K_f} \tag{7}$$

where,

$$K_f = \frac{2C_f^2 A_f^2}{\rho} \tag{8}$$

where C_f is the flow coefficient for the fixed orifice and A_f is the area of the fixed orifice.

So that for blocked port mode, i.e. when $Q_1 = 0$:

$$K_v x_{N1}^2 (P_1 - P_R) = (P_S - P_1) K_f \tag{9}$$

and rearranging gives:

$$P_1 = \frac{P_S K_f + P_R K_v \left(x_f - x_t\right)^2}{K_v \left(x_f - x_t\right)^2 + K_f} \tag{10}$$

Similarly it can be shown that P_2 can be expressed as:

$$P_2 = \frac{P_S K_f + P_R K_v \left(x_f + x_t\right)^2}{K_v \left(x_f + x_t\right)^2 + K_f} \tag{11}$$

The flow force will be small [27], so the fluid force acting on the nozzle target can be approximated as, (12)

$$F_N = \frac{\pi D_N^2}{4}(P_1 - P_2)$$

Equations (1) and (10) to (12) can be solved numerically to predict displacement and force at the nozzle target, as well as pressure at the two control ports, for any given control voltage in the blocked ports mode.

When the control ports are connected, $P_1 = P_2$, and equation (5) can be equated to the equivalent equation for port 2, giving:

$$\frac{Q_{N2}}{x_{N2}} = \frac{Q_{N1}}{x_{N1}} \tag{13}$$

Similarly from equation (7):

$$Q_1 + Q_{N1} = Q_2 + Q_{N2} \tag{14}$$

Equation (14) simply states that the flows through the two fixed orifices are the same when the two control port pressures are the same. Substituting for Q_{N2}in equation (14) using (13) and noting that with connected ports $Q_1 = -Q_2$:

$$Q_{N1} = \frac{2x_{N1}}{x_{N2} - x_{N1}} Q_1 \tag{15}$$

or

$$Q_{N1} = \frac{x_{N1}}{x_t} Q_1 \tag{16}$$

Summing equations (5) and (7):

$$\frac{(Q_1 + Q_{N1})^2}{K_f} + \frac{Q_{N1}^2}{K_v x_{N1}^2} = P_S - P_R \tag{17}$$

And substituting for Q_{N1}using equation (16):

$$\frac{Q_1^2}{x_t^2}\left(\frac{(x_t + x_{N1})^2}{K_f} + \frac{1}{K_v}\right) = P_S - P_R \tag{18}$$

Finally, substituting for x_{N1}using equation (4), the control flow in the connected ports case can be found as:

$$Q_1 = -Q_2 = x_t \sqrt{\frac{P_S - P_R}{\frac{{x_f}^2}{K_f} + \frac{1}{K_v}}} \tag{19}$$

Or in terms of flow coefficients:

$$Q_1 = -Q_2 = \sqrt{\frac{1}{\left(\frac{C_v \pi D_N x_f}{C_f A_f}\right)^2 + 1}} C_v \pi D_N x_t \sqrt{\frac{2(P_S - P_R)}{\rho}} \tag{20}$$

Thus the control port flow is proportional to the target displacement.

Table 3 shows the values used in the model including the constants for the ring bender performance K_1 and K_2 , the fixed and variable orifice diameters D_f and D_N, the coefficients of flow through the orifices C_f and C_v supplied by Rolls-Royce, the fluid density ρ, and the supply and return pressures P_S and P_R.

Parameter	**Value**
Ring bender voltage constant, K_1	0.75 μmV^{-1}
Ring bender compliance, K_2	5.77 μmN^{-1}
Nozzle target clearance, x_f	50 μm
Nozzle diameter, D_N	1 mm
Fixed orifice area, A_f	0.113 mm^2
Fixed orifice flow coefficient, C_f	0.9
Nozzle flow coefficient, C_v	0.65
Fluid density, ρ	870 kgm^{-3}
Supply pressure, P_S	varied: 30 to 110 bar
Return pressure, P_R	10 bar

Table 3. Model parameter values

4. Experimental results

4.1 Test overview

Three types of test were conducted:

- **i.** Blocked port tests, to determine the variation in pressure at ports 1 and 2 when there is no flow in or out of the ports, conducted at several supply pressures.
- **ii.** Connected port tests, to determine the variation in flow through ports 1 and 2 when they are connected together, so that the pressure at the ports is equal, conducted at several supply pressures.
- **iii.** A dynamic test, to determine the speed of response of the actuator.

The following signals were sampled at 1 kHz during the tests: the displacement of the nozzle target, the ring bender driving voltage (i.e. the amplifier output), and the pressures at port 1, port 2, supply and return. The flow between ports 1 and 2 was also measured in the connected port test using a gear flowmeter.

Note that, due to an amplifier offset, in the test results the control voltage varies between -92V and +106.5V rather than the nominal +/-100V, leading to a slightly asymmetrical displacement. Cyclic compression tests conducted with the fluorosilicone O-rings showed that they reduce in stiffness during the first few cycles converging quickly to a repeatable result [28]. Thus, it has been observed that the displacement of the ring bender increases slightly, about 5µm, after the first 3-4 tests, as the elastomer is cycled. The stiffness of the O-rings also decreases as the temperature increases which is discussed in Section 5. Thus test results were obtained when the oil temperature had stabilised at approximately 50°C.

It was observed in the initial valve calibration tests that the null position of the ring bender moved when the return pressure increased and this caused the valve to expand (by about 10µm with 15 bar return pressure), even though the valve body was designed to be very stiff. The expansion causes the distance from the eddy current sensor to the target to increase, and also the distance between the two nozzles to increase. Thus, the nozzle positions need to be adjusted for different return pressures to keep the nozzle clearance on both sides the same.

4.2 Blocked port results

With blocked ports pressures P_1 and P_2 were measured with a 1Hz triangular wave actuator drive signal at maximum amplitude (±100V). Figures 21 and 22 show 30 cycles superimposed for two different supply pressures. Both are with a dual lane configuration, with one driven actuator and one open circuit actuator; this replicates the condition where the second actuator has either failed or is in standby mode. The drive signal was chosen to be sufficiently slow such that dynamic effects were negligible.

Note that the dual lane arrangement with one inactive bender is expected to approximately double the stiffness of the combined actuator and thus reduce the free displacement by a factor of two compared with single lane mode. In fact, with an open circuit inactive actuator, when the driven ring bender displaces and causes the inactive ring bender to deform, an electric field will be developed in the inactive bender due to the piezoelectric effect, causing its effective stiffness to increase. Thus, the displacement is reduced further, and is a worse case than a short circuited inactive actuator. The

measured free displacement range with one open circuit ring bender is +/-75µm. For the dual lane tests the nozzles were positioned to allow the ring bender to move +/-50µm before nozzle contact, and thus at full displacement the actuator retained the capacity to exert a force and thus to resist fluid forces.

In Figures 21 and 22, which are for 30bar and 110bar supply pressures respectively, the actuator displacement and the pressures at the two control ports generally vary as expected. The return pressure is 10bar in both cases. As the ring bender displaces and moves the nozzle target towards port 1 the pressure at port 1 rises and the same for port 2. The pressure recovery, defined as the difference in control port pressures divided by the difference between supply and return pressures, peaks at 50% in Figure 21 and 40% in Figure 22. At the lower pressure, full displacement (+/-50µm) is reached at 75V on average, but 95V is required at the higher pressure due to the higher fluid force. Both plots show some asymmetry in the pressure curves for the two control ports, thought to be due to leakage around the port 1 adjuster, within the port 1 adjuster bore, and nozzle misalignment giving different closing characteristics. Hysteretic behaviour is clearly evident in two respects: hysteresis in the ring bender displacement is about 10% on average, and the hysteresis in the pressure vs. displacement plots is about 4bar. The former is the well-known piezoelectric hysteresis behaviour for actuators driven by voltage amplifiers [6]. The latter is probably due to the Coanda effect [29].

It can be seen that there is a reasonable correlation between the predicted and experimentally determined values for displacement and pressure for both the low and high pressure tests. The model does not include either source of hysteresis. To account for the asymmetrical pressure curves the return pressure terms and position offset were adjusted such that the return pressure for P_2 was increased to 12bar and there were 35µm and 48µm offsets on nozzles 1 and 2 respectively. These values account for different amounts of leakage around the nozzles and increased flow restriction for nozzle 2 flow path due to the asymmetrical structure of the flow paths through the valve.

Single lane tests, with just one actuator fitted into the valve, were also carried out. Nozzle positions were set to give a nozzle target displacement of +/-75µm, the increased displacement allowed by the reduced stiffness of the actuator module. This allowed the minimum port pressure to be reduced, giving a larger pressure swing at the control port: for example, the pressure recovery increases from 50% to 60% in the 30bar test equivalent to Figure 21; results can be found in [28].

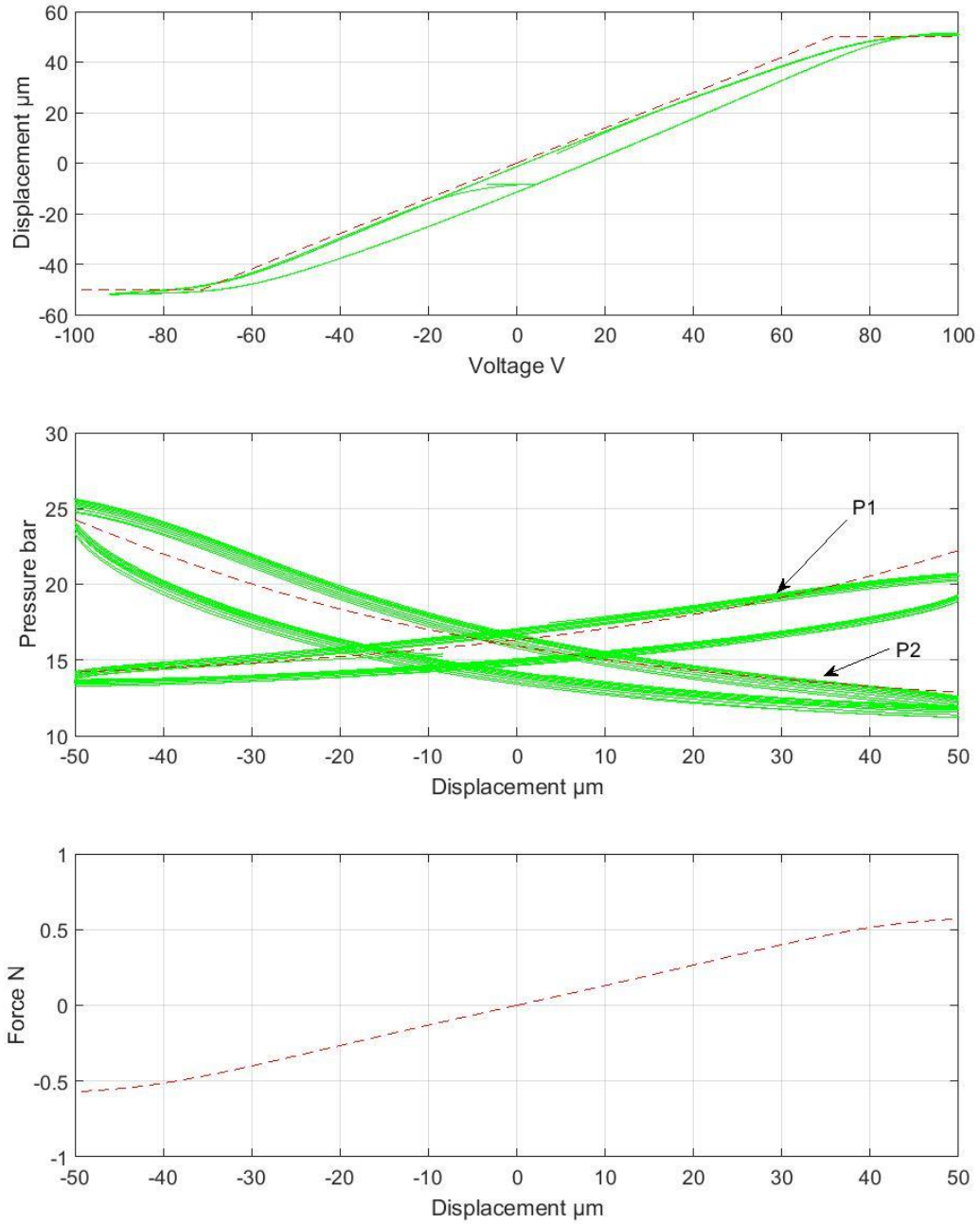

Figure 21. Comparison of model prediction and experimental results for dual lane test at supply pressure 30 bar, return pressure 10 bar with blocked ports. Nozzle clearance was +/-50µm. The dashed lines show the model predictions.

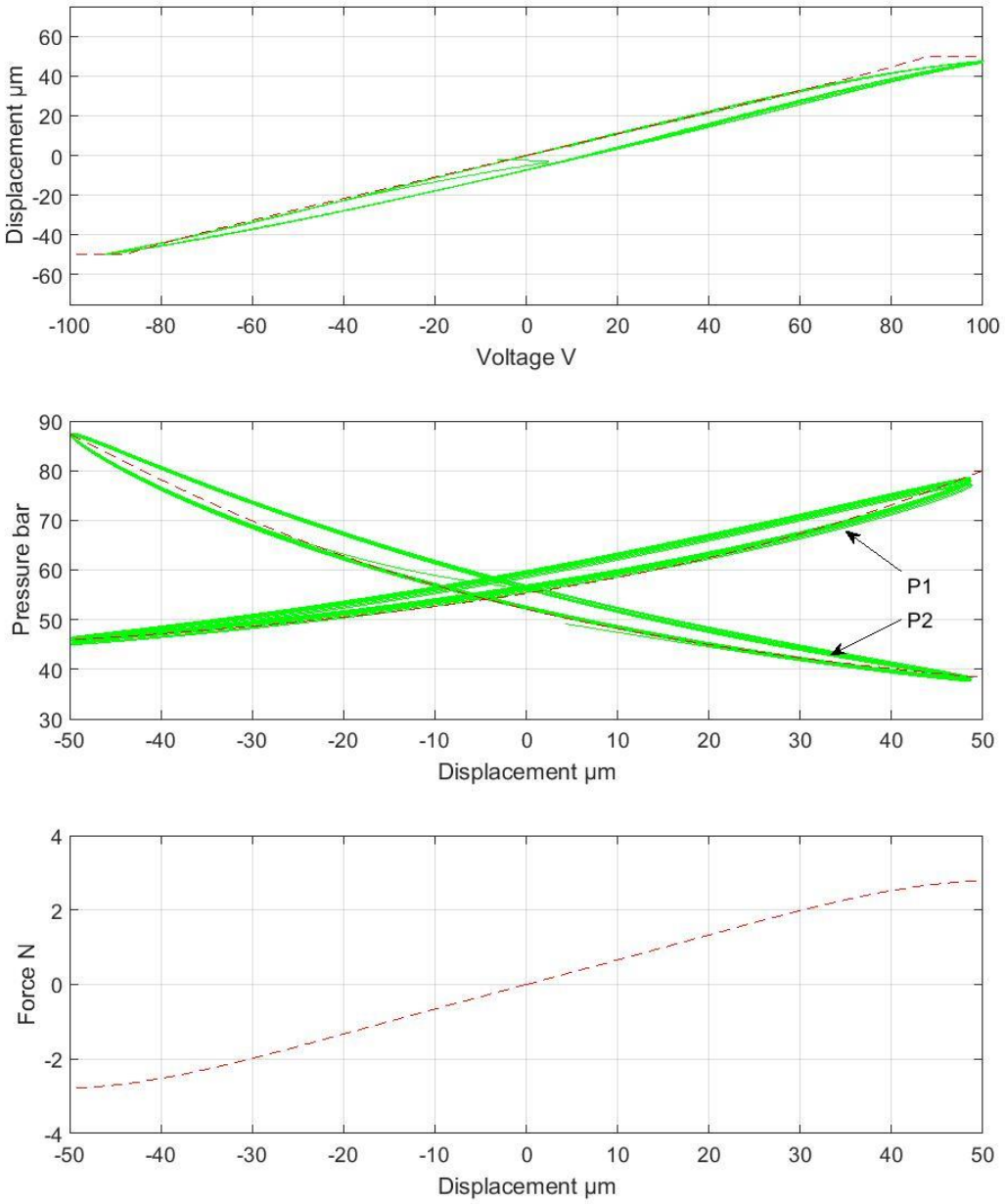

Figure 22. Comparison of model prediction and experimental results for dual lane test at supply pressure 110 bar, return pressure 10 bar with blocked ports. Nozzle clearance was +/-50µm. The dashed lines show the model predictions.

4.3 Connected port mode results

In the connected port tests, port 1 and 2 are connected together via a flowmeter. Figures 23 and 24 show how the flow between port 1 and port 2 varies with time when a triangle wave voltage of amplitude 100V is applied to the ring bender at a frequency of 0.025Hz. The supply pressure was 30bar and 110bar respectively, and the return pressure was 10bar. The flow between the flow ports is as expected and changes direction as the nozzle target moves past the null point. The data has been filtered to remove noise from the flow sensor. The non-linear behaviour shown around the zero flow region is due to the inaccuracy of the flow meter at low flow rates. In Figure 23 the maximum flow is 0.27 L/min (although less in the negative direction) and the flow gain at is 0.004L/min/V. In Figure 24 the maximum flow is 0.62 L/min and the flow gain at is 0.008L/min/V. The flows recorded are close to the predictions from the derived model. For example the match for the high pressure test is shown in Figure 25.

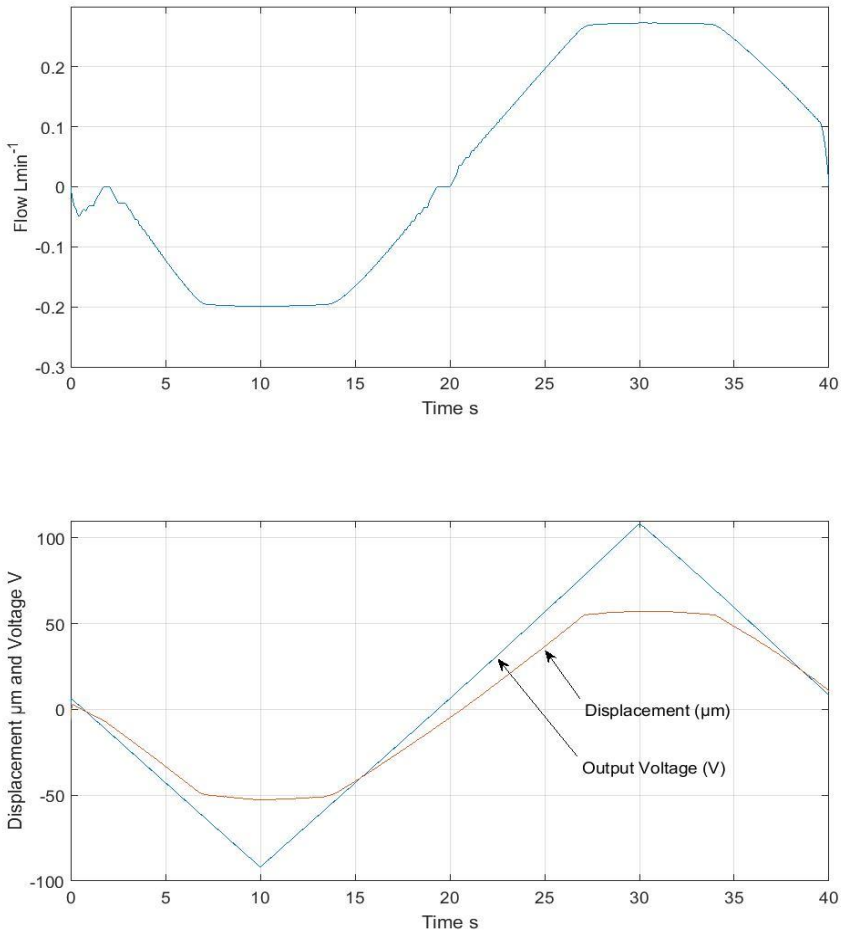

Figure 23. Connected ports: actuator displacement and flow (dual lane arrangement with nozzle clearance of +/-50µm). Supply pressure 30 bar, return pressure 10 bar.

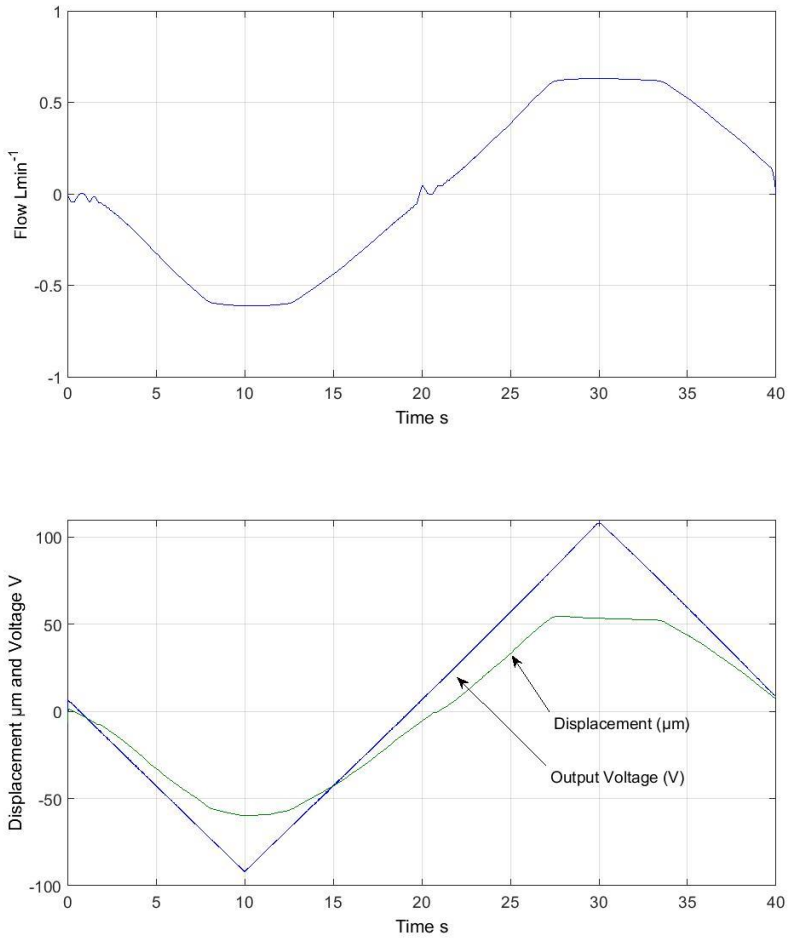

Figure 24. Connected ports: actuator displacement and flow (dual lane arrangement with nozzle clearance of +/-50µm). Supply pressure 110 bar, return pressure 10 bar.

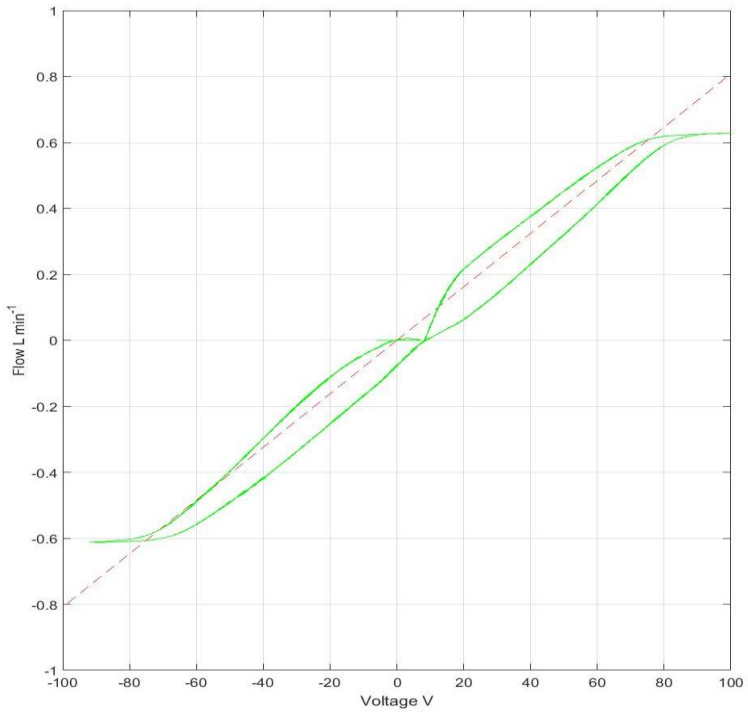

Figure 25. Comparison of experimental and predicted flow vs voltage at supply pressure 110 bar, return pressure 10 bar. Nozzle clearance was +/-50µm. The dashed line shows the model prediction.

4.4 Dynamic response

The dynamic response test was conducted in dual lane mode in air. A square wave was applied to the input of the amplifier to measure the response speed. Figure 26 shows the amplifier output voltage and the nozzle target displacement. Note that higher damping would be expected if operating in fuel or oil. In the first 0.5ms the nozzle target moves 92µm, giving a velocity of 18.4mm/s. The amplifier can be seen to be the most significant factor in reducing the speed of response. The rate of change of amplifier voltage is constrained due to its maximum current limit, linked to the capacitance of the ring bender. The gradient of the output voltage can be used to estimate the maximum current delivered by the amplifier. Based on the manufacturer's value for ring bender capacitance, 2 x 800nF, the maximum current is 80mA.

The stiffness of the mounted ring bender and the moving mass can be used to estimate the natural frequency observed in Figure 26. The stiffness is $1/K_2$ (see Table 3), which has the value 0.17×10^5 N/m. The mass of the nozzle target is 23.6g, and 7g is included in the lumped moving mass to account for part of the mass of each ring bender and also the inner edge mounting. Then the frequency can be estimated using:

$$f = \frac{1}{2\pi}\sqrt{\frac{1}{mK_2}}$$

This gives a natural frequency of 338Hz, which is reasonably consistent with Figure 26, which shows oscillation at about 320Hz.

For this application, a flapper actuation bandwidth of 200Hz is required [28], thus the results indicate that this is achievable. In fact the mass of the nozzle target in the prototype valve could be significantly reduced in future versions, which would further increase the natural frequency, and also bandwidth especially if coupled to a fast-response high-current amplifier.

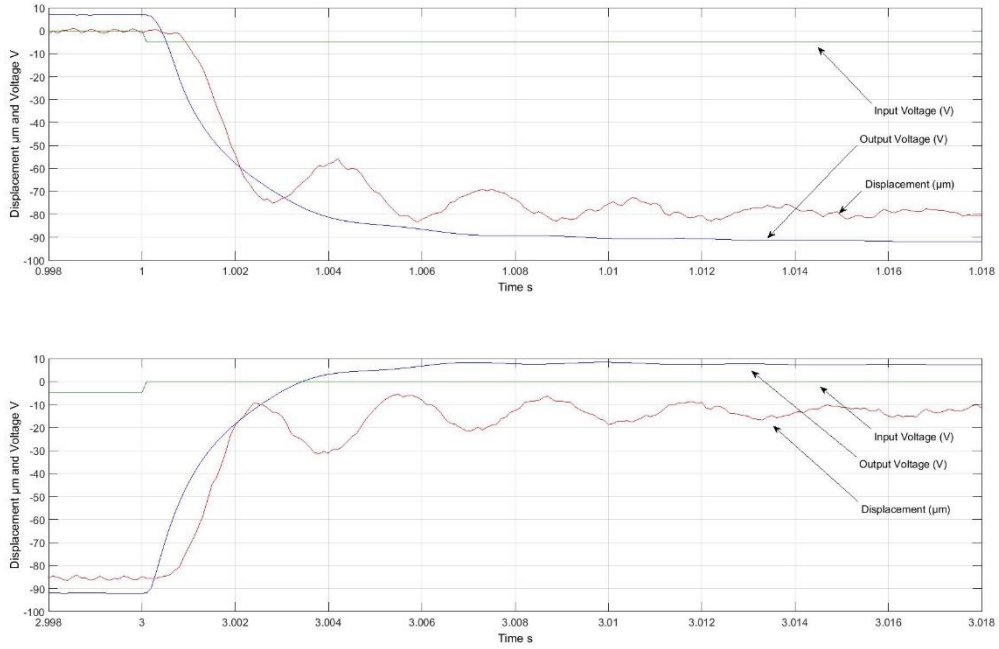

Figure 26. Response for step input of -100V amplitude. Test conducted dry.

5. Conclusions

A novel piezoelectric nozzle-flapper servovalve was designed, modelled, built and tested. The investigation focussed on determining the suitability of the concept as a pilot stage in an aero engine fuel metering valve, as an alternative to the tradition nozzle-flapper pilot stage actuated by an electromagnetic torque motor. Redundancy is required in this application, and thus two piezoelectric ring benders were built into the valve, and the characteristics tested when only one of the ring benders was active to simulate a failure condition.

The pressures at the two output (control) ports of the valve were recorded when the ports were blocked and the flow between them was recorded when they were connected. The experimental results for cycling the ring bender voltage through full range were compared to the predictions of an analytical model and a good correlation was observed for the two supply pressures presented (30bar and 110bar). The nozzles are positioned to allow a flapper stroke of ±50µm, and in the higher supply pressure tests the pressure recovery (output pressure swing over input pressure difference) is 40% in blocked port mode, and the maximum flow rate is 0.61L/min with connect ports. These results indicate that the device could be feasible as the pilot stage in a fuel metering valve. The reduced actuator stiffness in single lane tests, with a single ring bender, means that ±75µm flapper stroke is possible giving increased valve performance, but at the expense of no redundancy [28]. The pressure

recovery could probably be improved with tighter manufacturing tolerances; it is likely there is significant leakage through the nozzle even when it is 'closed', for example due to angularity error preventing the flapper from properly abutting the nozzle. Ideally, ±75μm needs to be achieved in the dual lane device, and studies indicate that this should be possible with larger ring benders [28].

The steady state analytical model predicts the scale and trends of pressure and flow variation with voltage reasonably well, for example accurately predicting a flow gain of $8mLmin^{-1}V^{-1}$. The ring bender displacement is modelled as a weighted sum of the applied voltage and the resultant fluid force acting on the target due to the nozzles, and the orifice equation is applied to the fixed and variable H-bridge orifices. However hysteresis is not included in the model, and this causes discrepancies with the experimental results both for the voltage-displacement relationship (piezoelectric hysteresis) and the displacement-pressure or displacement-flow relationship. In the physical device, implementation of a method to compensate for hysteresis, such as that described in [26] would be beneficial.

The dynamic response is demonstrated by applying a zero to maximum voltage step to the ring bender amplifier. The ring bender shows a phase delay of about 0.6ms with respect to the amplifier output voltage, followed by a lightly damped oscillation at 340Hz. However the amplifier output voltage response is slower, with a time constant of about 1.6ms. This dynamic response is adequate for the intended application. It could be improved by using a fast-response high-current amplifier, and reducing the mass of the target carried by the ring bender. Note that the results shown were carried out dry (in air), and the response exhibits more damping in a wet test.

A challenge in the design of a ring bender actuated device is the mounting of the ring bender, which has to flex to allow the outer edge of the ring bender to rotate, yet be stiff enough axially to adequately react generated forces. Elastomer O-rings have been investigated and successfully applied to mount the ring benders used in this work. Note that a highly repeatable assembly process is required to ensure consistent overlap between the O-ring mounts and the ring bender. In aerospace, an added complication is the large range of temperatures, and F70 fluorosilicone O-rings have been chosen with this in mind, and successfully used to mount a ring bender tested actively between -50°C to +180°C. However, it is known that F70 fluorosilicone absorbs liquids (e.g. fuel or oil) and swells after prolonged exposure leading to variation in properties such as size of the contact region and stiffness. This issue requires further investigation. Other reliability concerns that have not been investigated in this work are the effect of long term exposure of the piezoelectric actuator to fuel – which would probably necessitate encapsulation of the actuator – and the robustness of electrical connections.

In comparison with the other piezoelectric actuator types investigated for valve pilot stage actuation as reviewed in Section 1.2, ring benders have a very appropriate balance between output force and displacement range. Stack actuators of sufficient compactness provide too small a displacement, noting that the useable displacement is much less than the free displacement due to loading and thermal expansion, and so mechanical amplification is required to allow adequate orifice opening. Flexure-based mechanical amplification is possible but this reduces the maximum energy-per-stroke output of the actuator due to the flexure strain energy, and increases size and mass which in turn reduces dynamic response. Bi-directional three-wire multi-layer bending actuators are now widely available which require fairly modest drive voltages (sub-100V), and their electric field is always

applied in the poling direction and so field strength is not constrained by the danger of depolarisation. However rectangular benders have struggled to give sufficient force output for valve pilot stage actuation. Ring benders on the other hand can harness a larger volume of ceramic to drive their inner edge relative to their outer edge, and also harness strain in both the d_{31} and d_{32} in-plane directions to deform the ring. The consequence is that larger blocking forces can be generated, typically in the region of 10's of newtons. A key challenge however is the mounting of the ring bender to allow it to both deform and react a load, as addressed in this paper.

This research establishes that a piezoelectric aero engine fuel valve is feasible, replacing the traditional electromagnetic transduction in the pilot stage of the valve. In particular, it is shown that piezoelectric ring bender actuators are highly suited to this application, and that elastomeric ring bender mounting is effective. This new approach opens up the possibility of reducing manual operations in manufacture, improving repeatability, and eliminating failures associated with fine wire devices.

Acknowledgement
The research presented was collaborative between the University of Bath and Rolls-Royce plc, and partially funded by the Engineering and Physical Sciences Research Council (EPSRC) via a Co-operative Award in Science and Engineering (PhD CASE award).

References

1. Airbus, 2018, "Global Market Forecast: Global Networks, Global Citizens 2018-2037", Airbus S.A.S., Reference D14029465, Issue 5. August, 2018.
2. Hansen, L.D., Kucera, G.D., Clemons, J.S. and Lee, J. 1997. "Aircraft gas turbine engine fuel pumping systems in the 21st century", *Journal of Engineering for Gas Turbines and Power*, Vol.119, pp 591-597
3. Delphi. *Piezoelectric Injector.* [online] Available at: < www.delphi.com> [Accessed 2017]
4. Schiller, N.H., Saunders, W.R., Chishty, W.A., Vandsburger, U. and Baumann, W.T., 2006, "Development of a piezoelectric-actuated fuel modulation system for active combustion control", *Journal of Intelligent Material Systems and Structures*, vol. 17, pp 403-410
5. Bertin, M.J.F., Plummer, A. R., Bowen, C. R., and Johnston, D. N., 2014, "An investigation of piezoelectric ring benders and their potential for actuating servovalves." *Bath/ASME Symposium on Power Transmission and Motion Control FPMC2014, Bath,*
6. Hall, D., A., 2001, "Review of nonlinearity in piezoelectric ceramics", *J. Mater. Sci.* vol. 36, pp. 4575–4601.
7. Boyar. R. E., Johnson, B. A., and Schmid, L., "Hydraulic Servo Control Valves Part 1", *WADC Technical Report 55-29*, Wright-Patterson Air Force Base, Ohio, 1955.
8. Johnson, R., Stahl, R., and Walters, G. (Textron Inc) Non-magnetic electro-hydraulic transfer valve. Patent US2928409. Filed Jan 1955, granted Mar 1960.
9. Tamburrano P, Plummer AR, Distaso E, Amirante R, 2018 "A review of electro-hydraulic servovalve research and development", International Journal of Fluid Power, October 2018.
10. Plummer, A.R., 2016, "Electrohydraulic servovalves - past, present, and future", Proc. 10th Int. Fluid Power Conf., Dresden, March 2016
11. Karunanidhi, S., and Singaperumal, M., 2010, "Mathematical modelling and experimental characterization of a high dynamic servo valve integrated with piezoelectric actuator", *Proc. Inst. Mech. Eng. Part J. Syst. Control Eng.* vol. 224, , pp.419–435.

12. Sangiah, D., Plummer, A. R., Bowen, C. and Guerrier, P., “A novel piezohydraulic aerospace servovalve. Part I : Design and modelling”. *Proceedings of the Institution of Mechanical Engineers, Part I: Journal of Systems and Control Engineering*, 227 (4), 2014, pp. 371-389.
13. Milecki, A., 2006, "Modelling and investigations of electrohydraulic servo valve with piezo element", *Archiwum Technologii Maszyn i Automatyzacji*, Vol.26, Nr.2
14. Persson, L.J., Plummer, A.R., Bowen, C., and Brooks, I. Design and Modelling of a Novel Servovalve Actuated by a Piezoelectric Ring Bender. Proc ASME/Bath Symposium on Fluid Power and Motion Control, Chicago, October 2015.
15. Persson, L.J., Plummer, A.R., Bowen, C., and Brooks, I., 2016 , “A lightweight, low leakage piezoelectric servovalve.” *Recent Advances in Aerospace Actuation Components and Systems 2016 (R3ASC'16),*
16. Persson, L.J., Plummer, A., Bowen, C., and Elliott, P., 2017, "Nonlinear Control of a Piezoelectric Two Stage Servovalve" in *Proceedings of 15th Scandinavian International Conference on Fluid Power*, June 7-9, 2017, Linköping, Sweden.
17. Hagemeister, W., 1999. “Auslegung von hochdynamischen servohydraulischen Antreiben fur eine active Frasspindellagerung.*” Aachen: RWTH.*
18. Bauer, F. and Reichert, M. 2005. "The use of piezo-actuators for high dynamic servovalves", *Olhydraulik and Pneumatik*, Vol.49, Nr.6
19. Tamburrano P, Amirante R, Distaso E, Plummer AR. A, 2018 “Novel Piezoelectric Double-Flapper Servovalve Pilot Stage: Operating Principle and Performance Prediction.” *BATH/ASME 2018 Symposium on Fluid Power and Motion Control*, Sept 2018, Bath UK.
20. Tamburrano P, Amirante R, Distaso E, Plummer AR. A, 2018 “Full simulation of a piezoelectric double nozzle flapper pilot valve coupled with a main stage spool valve,” Energy Procedia, Volume 148, Pages 487-494
21. Reichert, M. and Murrenhoff, H., 2006, “New Concepts and Design of High Response Hydraulic Valves Using Piezo-Technology.” *Power Transmission and Motion Control Symposium*, Sept 2016. Bath, UK.
22. Griffiths, M., 2007, “BR725 Fuel Metering Unit (FMU): Steady State Model and Performance Report Index, *Goodrich Engineering Report*.
23. Hooker, M.W., 1998, "Properties of PZT-Based Piezoelectric Ceramics Between -150 and 250°C ", *Lockheed Martin Engineering and Sciences Co. Hampton, Virginia, NASA/CR-1998-208708,* vol. 230:5
24. McCloy, D., Martin, H. R., 1980, “Control of fluid power: Analysis and design”, *Ellis Horwood, Chichester*.
25. Zhu, Y., and Fei, S., 2016, “Design Criterion Involving Comprehensive Performance Characteristics of Nozzle Flapper Valves”. *Part I: Journal of Systems and Control Engineering,* p452-466.
26. Stefanski, F., Minorowicz, B., Persson, J., Plummer, A. and Bowen, C., 2017, "Non-linear control of a hydraulic piezo-valve using a generalised Prandtl–Ishlinskii hysteresis model ", *Journal of Mechanical Systems and Signal Processing*, vol. 82, p412-431.
27. Merritt, H.E., 1967, “Hydraulic Control Systems”, *John Wiley & Sons, New York*
28. Bertin, M.J.F., 2017, “Piezoelectric actuation of an aero engine fuel metering valve”, Thesis, University of Bath
29. Tritton, D.J., Physical Fluid Dynamics, Van Nostrand Reinhold, 1977